Electronic Supporting Information

Luminescent Solar Concentrators Based on Energy Transfer from an Aggregation-Induced Emitter Conjugated Polymer

Guanpeng Lyu,[a] James Kendall,[a] Ilaria Meazzini,[a] Eduard Preis,[b] Sebnem Bayseç,[b] Ullrich Scherf,[b] Sébastien Clément,[c] Rachel C Evans[a]*

[a]Department of Material Science & Metallurgy, University of Cambridge, 27 Charles Babbage Road, Cambridge, CB3 0FS, U.K. Email: rce@cam.ac.uk

[b]Macromolecular Chemistry Group (buwmakro) and Institute for Polymer Technology, Bergische Universität Wuppertal, Gausss-Str. 20, D-42119 Wuppertal, Germany.

[c] Institut Charles Gerhardt Montpellier, ICGM, UMR 5253, CNRS, Université de Montpellier, ENSCM, Place Eugène Bataillon, 34095 Montpellier cedex 5, France.

*Corresponding author: rce26@cam.ac.uk

Table of Contents

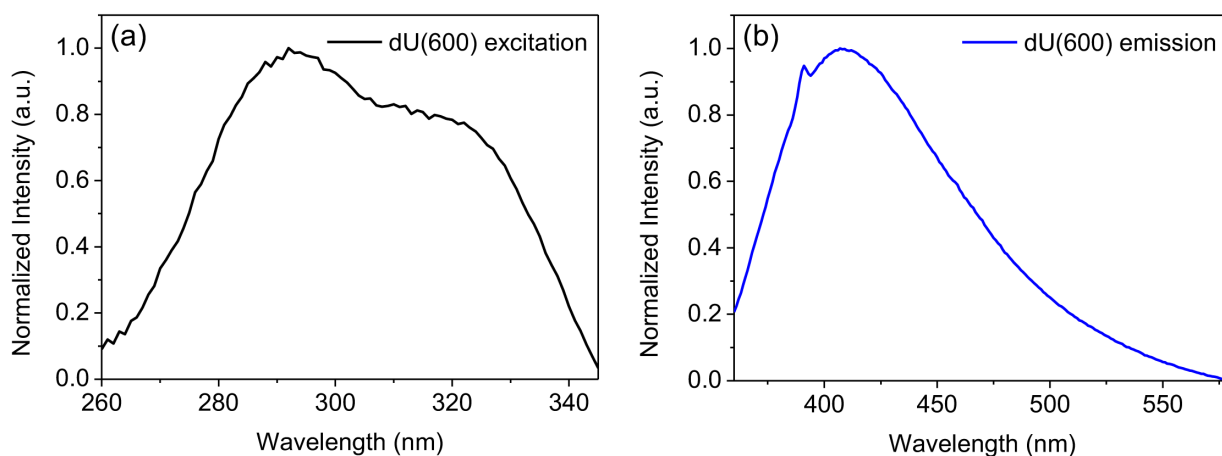# 1. Photoluminescence properties of dU(600) waveguides

Figure S1. (a) Photoluminescence excitation (λ_{em} = 360 nm) and (b) emission spectra (λ_{ex} = 350 nm) of dU(600) waveguides.

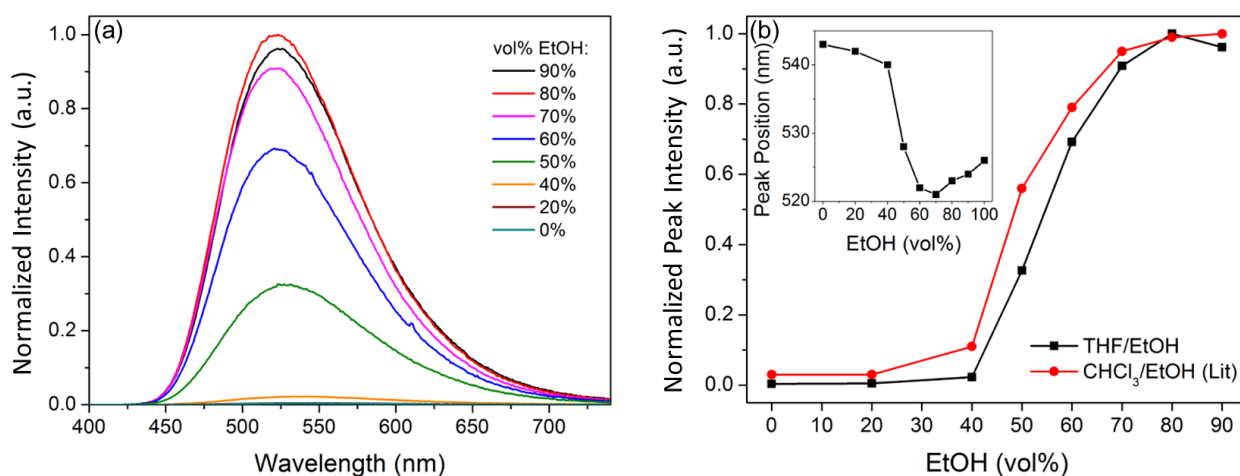# 2. Aggregation-induced emission (AIE) behaviour of p-O-TPE in THF/EtOH

Figure S2. (a) Emission spectra (λ_{ex} = 373 nm) of p-O-TPE in THF/EtOH solutions of varying EtOH concentration. (b) Variation of peak intensity of p-O-TPE emission (λ_{ex} = 373 nm) in THF/EtOH (black) and CHCl$_3$/EtOH (red)[1] with varying EtOH concentration. Inset: variation of peak position of p-O-TPE emission in THF/EtOH.

3. Steady-state photoluminescence studies of p-O-TPE-PDI-Sil energy transfer in dU(600)
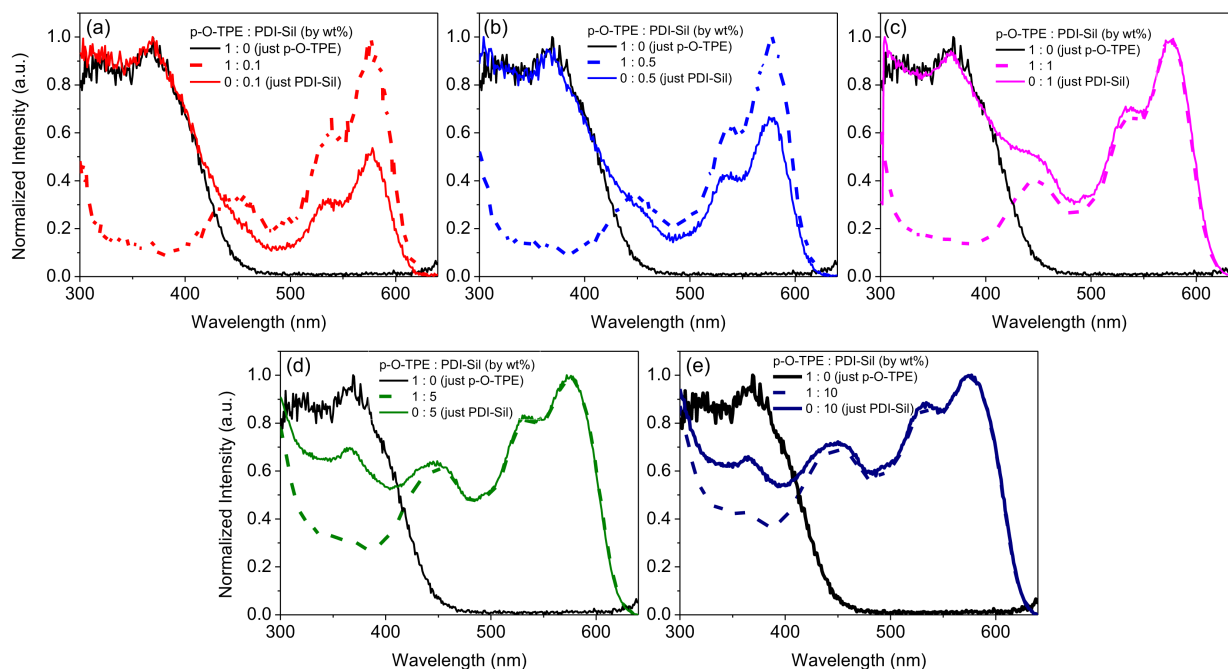
3.1 Excitation spectra

Figure S3. (a)-(e) Normalized excitation spectra (λ_{em} = 650 nm) of p-O-TPE-dU(600) (solid black), p-O-TPE-PDI-Sil-dU(600) (solid coloured) and PDI-Sil-dU(600) (dash coloured) with varying concentration ratios between p-O-TPE and PDI-Sil. A concentration ratio of 1 : 1 represents 0.005 wt% of p-O-TPE and 0.005 wt% of PDI-Sil.

3.2 Emission spectra

The enhancement in PDI-Sil emission as a result of FRET is calculated by comparing the PDI-Sil emission in p-O-TPE-PDI-Sil-dU(600) and PDI-Sil-dU(600) (Figure S4). Firstly, the p-O-TPE emission in p-O-TPE-dU(600) is normalized by the peak intensity of p-O-TPE emission in p-O-TPE-dU(600) (Figure S5). Subsequently, it is subtracted from the emission of p-O-TPE-PDI-Sil-dU(600) to get the emission of PDI-Sil in p-O-TPE-PDI-Sil-dU(600) and compared to the emission of PDI-Sil in PDI-Sil-dU(600) (Figure S6). The difference in integrated photon counts between the PDI-Sil emission in p-O-TPE-PDI-Sil-dU(600) and PDI-Sil-dU(600) corresponds to the increase in PDI-Sil emission due to FRET from p-O-TPE.
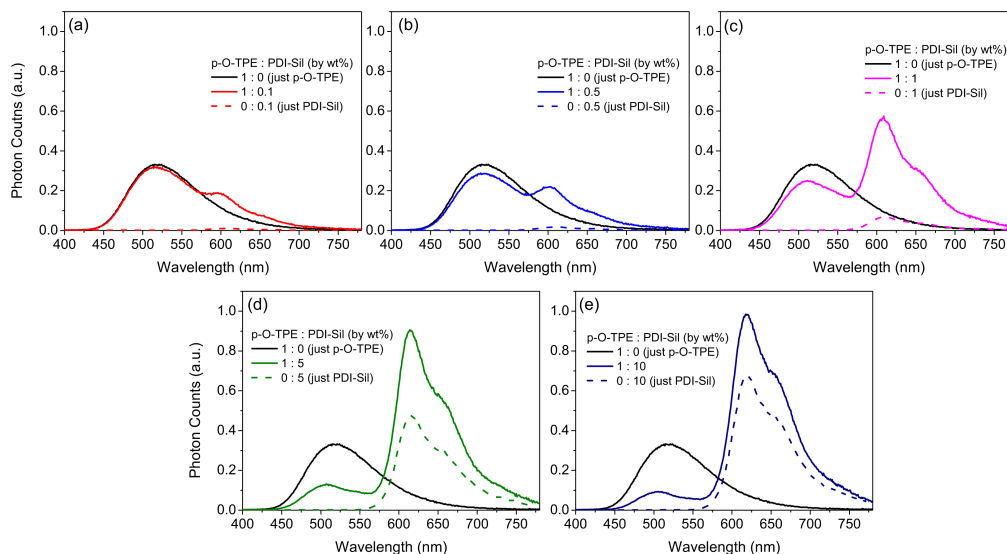
Figure S4. (a)-(e) Emission spectra (λ_{em} = 370 nm) of p-O-TPE-dU(600) (solid black), p-O-TPE-PDI-Sil-dU(600) (solid coloured) and PDI-Sil-dU(600) (dash coloured) with varying concentration ratios between p-O-TPE and PDI-Sil. A concentration ratio of 1 : 1 represents 0.005 wt% of p-O-TPE and 0.005 wt% of PDI-Sil.

Figure S5. (a)-(e) Emission spectra (λ_{em} = 370 nm) of p-O-TPE-dU(600) (solid black, normalized by the peak intensity of p-O-TPE emission in p-O-TPE-PDI-Sil-dU(600)), p-O-TPE-PDI-Sil-dU(600) (solid coloured) and PDI-Sil-dU(600) (dash coloured) with varying concentration ratios between p-O-TPE and PDI-Sil. A concentration ratio of 1 : 1 represents 0.005 wt% of p-O-TPE and 0.005 wt% of PDI-Sil.
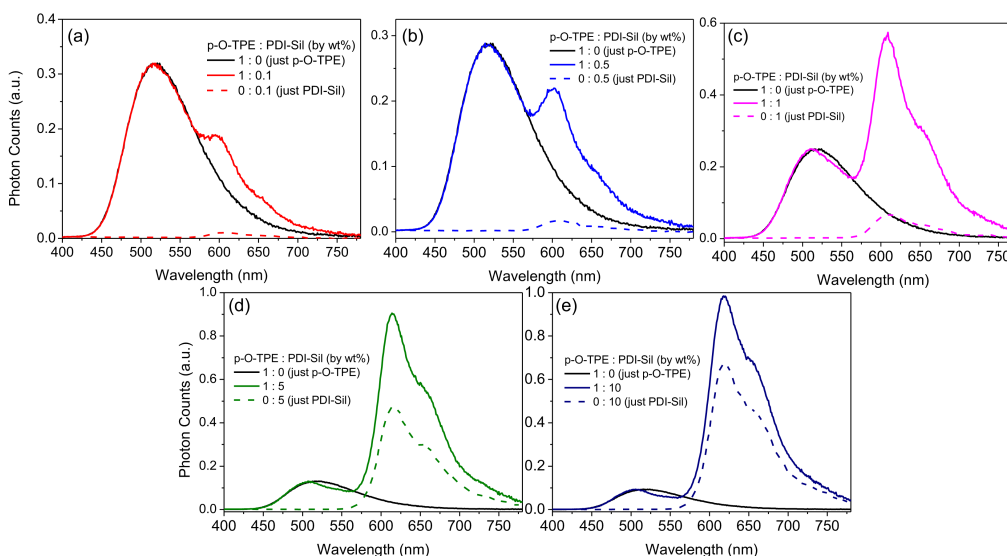
Figure S6. (a)-(e) Emission spectra (λ_{em} = 370 nm) of PDI-Sil in p-O-TPE-PDI-Sil-dU(600) (solid) and PDI-Sil-dU(600) (dash) with varying concentration ratios between p-O-TPE and PDI-Sil. A concentration ratio of 1 : 1 represents 0.005 wt% of p-O-TPE and 0.005 wt% of PDI-Sil.
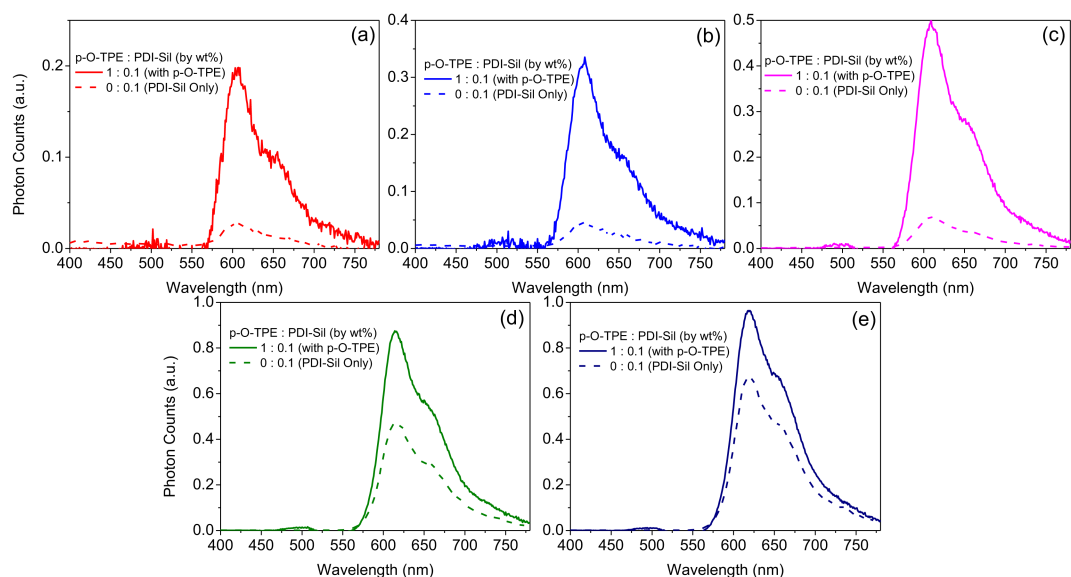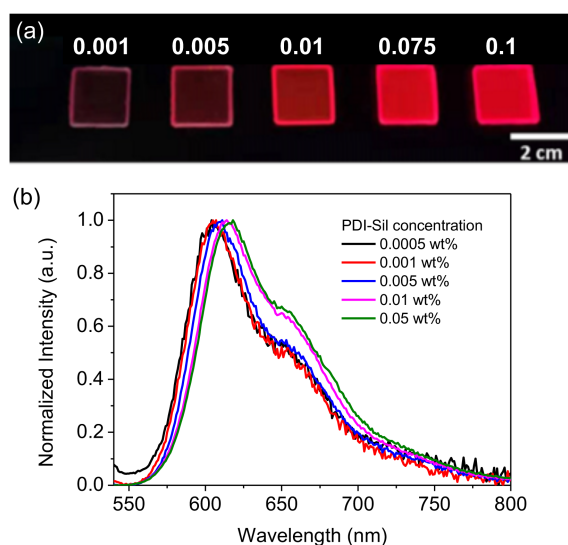

Figure S7. Optical properties of PDI-Sil-dU(600) ureasils. (a) Photograph of PDI-Sil-dU(600) samples doped with varying concentration of PDI-Sil under UV illumination (365 nm). The value above each sample represents the concentration (wt%) of PDI-Sil in dU(600). (b) Normalized emission spectra (λ_{ex} = 530 nm) of PDI-Sil-dU(600) samples with varying concentrations of PDI-Sil.

3.3 Integrated photon counts of edge emission
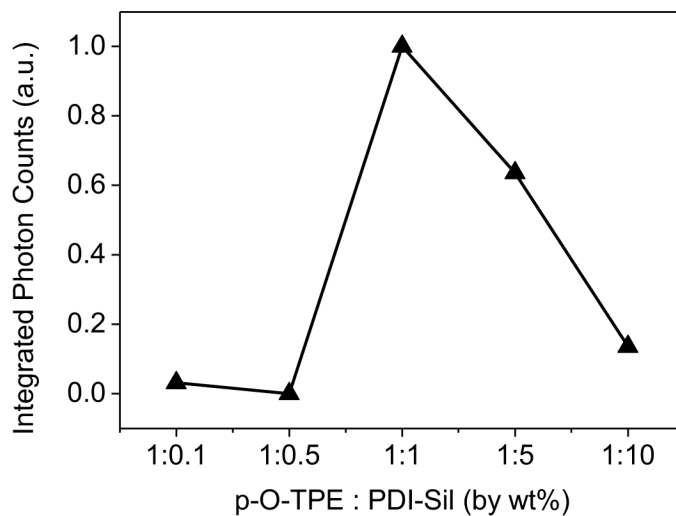

Figure S8. Number of photons emitted from the edge of p-O-TPE-PDI-Sil-dU(600) samples as a function of p-O-TPE : PDI-Sil concentration ratio in arbitrary units.

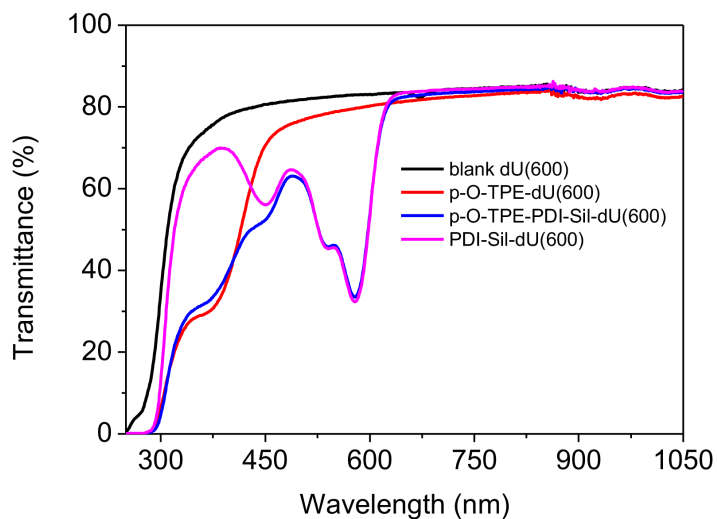## 4. UV/Vis transmittance and absorption spectra of large LSCs

Figure S9. UV/Vis transmittance spectra of dU(600), p-O-TPE-dU(600), PDI-Sil-dU(600) and p-O-TPE-PDI-Sil-dU(600) samples (4.5 cm × 4.5 cm × 0.3 cm).
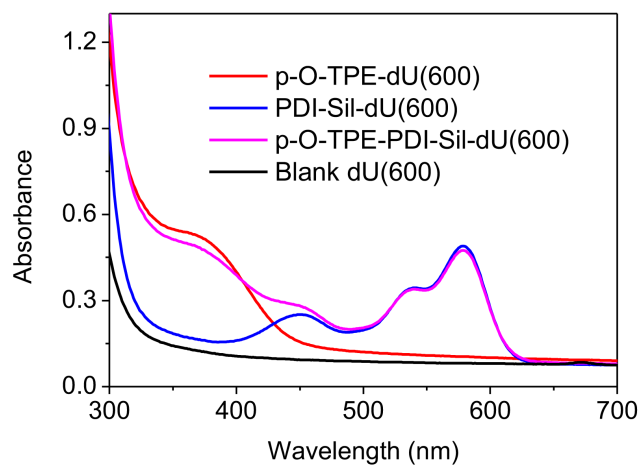
Figure S10. UV/Vis absorption spectra of dU(600), p-O-TPE-dU(600), PDI-Sil-dU(600) and p-O-TPE-PDI-Sil-dU(600) (4.5 cm × 4.5 cm × 0.3 cm).

5. Literature comparison of LSC efficiencies

Table S1. Performance metrics of the p-O-TPE-PDI-Sil-LSC reported in this work compared to some examples from the recent literature.

Type	Dimensions	Geometric Gain[a]	Light Source	η_{int}[b]
This work	4.5 cm × 4.5 cm × 0.3 cm	3.8	AM1.5G Solar simulator	20.0%
CdSe/ZnS core/shell-Alexa Fluor 546 dye[2]	4 cm × 4 cm × 0.27 cm	3.7	AM1.5G Solar simulator	19.8%
Silica-coated CdSe/CdZn$_x$S$_{1-x}$ core/alloyed shell[3]	10 cm × 10 cm × 0.16 cm	15.6	Sunlight	21.0%
Perovskite nanoplatelets[4]	10 cm × 10 cm × 0.2 cm	12.5	Sunlight	26.0%
PbS/CdS core/shell[5]	10 cm × 10 cm × 0.2 cm	12.5	Solar simulator	4.5%
CuInSeS$_2$In/ZnS core/shell[6]	10 cm × 10 cm × 0.3 cm	8.3	Solar simulator	16.7%
Silicon quantum dots[7]	12 cm × 12 cm × 0.26 cm	11.5	Solar simulator	30.0%
CdSe/CdS core/shell[8]	21.5 cm × 1.3 cm × 0.5 cm	1.2	Solar simulator	10.2%

[a] The geometric gain (G) of an LSC is defined by:

$$G = \frac{A_{top}}{A_{edge}} \tag{S1}$$

where A_{top} and A_{edge} are the areas of the top surface and edges of the LSC, respectively.

[b] The internal photon efficiency (η_{int}) of an LSC is defined by the following equation:

$$\eta_{int} = \frac{N_{ph-out}}{N_{ph-abs}} \tag{S2}$$

where N_{ph-out} is the total number of edge-emitted photons summed over four edges of the LSC and N_{ph-abs} is the total number of photons absorbed by the LSC.

6. References

[1]   Baysec, S.; Preis, E.; Allard, S.; Scherf, U., Very High Solid State Photoluminescence Quantum Yields of Poly (tetraphenylethylene) Derivatives. *Macromol. Rapid Commun.* **2016,** 37, 1802-1806.

[2]   Tummeltshammer, C.; Portnoi, M.; Mitchell, S.A.; Lee, A-T.; Kenyon, A. J.; Tabor, A. B.; Papakonstantinou, I., On the ability of Förster resonance energy transfer to enhance luminescent solar concentrator efficiency. *Nano Energy.* **2017,** 32, 263-270.

[3]   Li, H.; Wu, K.; Lim, J.; Song, H. J.; Klimov, V. I., Doctor-blade deposition of quantum dots onto standard window glass for low-loss large-area luminescent solar concentrators. *Nat. Energy.* **2016,** 1, 1-9.

[4]   Wei, M.; Arquer, F. P. G. D.; Walters G, Yang, Z.; Quan, L. N.; Kim, Y.; Sabatini, R.; Quintero-Bermudez, R.; Gao, L.; Fan, J. Z.; Fan, F.; Gold-Parker, A.; Toney, M. F.; Sargent, E. H., Ultrafast narrowband exciton routing within layered perovskite nanoplatelets enables low-loss luminescent solar concentrators. *Nat. Energy.* **2019,** 4, 197-205.

[5]   Zhou, Y.; Benetti, D.; Fan, Z.; Zhao, H.; Ma, D.; Govorov, A. O.; Vomiero, A.; Rosei, F., Near Infrared, Highly Efficient Luminescent Solar Concentrators. *Adv. Energy Mater.* **2016,** 6, 1–8.

[6]   Meinardi, F.; McDaniel, H.; Carulli, F.; Colombo, A.; Velizhanin, K. A.; Makarov, N. S.; Simonutti, R.; Klimov, V. I.; Brovelli, S., Highly efficient large-area colourless luminescent solar concentrators using heavy-metal-free colloidal quantum dots. *Nat. Nanotechnol.* **2015,** 10, 878–885.

[7]   Meinardi, F.; Ehrenberg, S.; Dhamo, L.; Carulli, F.; Mauri, M.; Bruni, F.; Simonutti, R.; Kortshagen, U.; Brovelli,S., Highly efficient luminescent solar concentrators based on earth-Abundant indirect-bandgap silicon quantum dots. *Nat. Photonics* **2017,** 11, 177–185.

[8]   Meinardi, F.; Colombo, A.; Velizhanin, K. A.; Simonutti, R.; Lorenzon, M.; Beverina, L.; Viswanatha, R.; Klimov, V. I.; Brovelli, S., Large-area luminescent solar concentrators based on Stokes-shift-engineered nanocrystals in a mass-polymerized PMMA matrix. *Nat. Photonics.* **2014,** 8, 392-399.